International Journal of Fracture (2005) 132:223–248
DOI 10.1007/s10704-005-2181-2

Analysis of beam-type fracture specimens with crack-tip deformation

JIALAI WANG[1] and PIZHONG QIAO[2,*]
[1] *Department of Civil Engineering and Construction, North Dakota State University, ND 58105-5285, USA*
[2] *Advanced Materials and Structures Research Group, Department of Civil Engineering, The University of Akron, Akron, OH 44325-3905, USA*
[*] *Author for correspondence (E-mail address: qiao@uakron.edu)*

Received 8 September 2004; accepted in revised form 14 February 2005

Abstract. A novel bi-layer beam model is developed to account for local effects at the crack tip of a bimaterial interface by modeling a bi-layer composite beam as two separate shear deformable beams. The effect of interface stresses on the deformations of sub-layers, which is referred to as the elastic foundation effect in the literature, is considered in this model by introducing two interface compliance coefficients; thus a flexible joint condition at the crack tip is considered in contrast to the "rigid joint" condition used in the conventional bi-layer model. An elastic crack tip deformable model is presented, and the closed-form solutions of local deformation at the crack tip are then obtained. By applying this novel crack tip deformation model, the new terms due to the local deformations at the crack tip, which are missing in the conventional composite beam solutions of compliance and energy release rate (ERR) of beam-type fracture specimens, are recovered. Several commonly used beam-type fracture specimens are examined under the new light of the present model, and the improved solutions for ERR and mode mixity are thus obtained. A remarkable agreement achieved between the present and available solutions illustrates the validity of the present study. The significance of local deformation at the crack tip is demonstrated, and the improved solutions developed in this study provide highly accurate predictions of fracture properties which can actually substitute the full continuum elasticity analysis such as the finite element analysis. The new and improved formulas derived for several specimens provide better prediction of ERR and mode mixity of beam-type fracture experiments.

Key words: Compliance, crack tip deformation, energy release rate, fracture specimens, improved data reduction, mode mixity, transverse shear deformation.

1. Introduction

Beam-type fracture specimens (Davies et al., 1998) are widely used to study the interlaminar delamination, one of the most common failure modes in layered structures such as laminated composites. A compliance approach is commonly used to determine the energy release rate (ERR) and mode mixity of the beam-type fracture specimens and develop the related data reduction procedures. In this method, the ERR of the specimen is calculated through the derivative of compliance; while the compliance is obtained through modeling the specimen as a split beam, i.e., the cracked portion is modeled as two separate beams and the virgin portion is modeled as a composite beam. At the crack tip where a joint is formed connecting the

cracked and virgin parts of the specimen, the cross-sections of the beams are assumed to remain in one plane and perpendicular to the mid-plane of the virgin part. Thus, the elastic deformation such as the differential extension and root rotation at the crack tip is neglected (Sun and Pandey, 1994), and a "rigid joint" is formed. Such a rigid joint beam model under-evaluates the compliance of the specimen and predicts a relatively approximate ERR of the specimen.

Extensive efforts have been made to find better equations to determine the ERR and mode mixity of beam-type specimens, which essentially are to account for the local deformation at the crack tip. Sun and Pandey (1994) obtained an approximate two dimensional elastic solution of root rotation at the joint (crack tip) of an isotropic and materially homogeneous split beam. Sundararaman and Davidson (1998) used a torsional spring to describe the deformation at the joint in order to obtain reasonably accurate results in their analysis of an unsymmetric end-notched flexure (ENF) specimen, in which the stiffness of the torsional spring was obtained numerically. Shu and Mai (1993) used both the "rigid" and "soft" joint models to evaluate the upper and lower bounds of buckling and vibration of bimaterial split beam. A better solution of compliance and ERR with consideration of local deformation at the crack tip (Williams, 1989; Wang and Williams, 1992; Corleto and Hogan, 1995; Ozil and Carlsson, 1999; Qiao et al., 2003a,b) was obtained by using a beam on elastic foundation model pioneered by Kanninen (1973, 1974) and the local deformation was captured as the "elastic foundation effect" with two foundation stiffness coefficients. However, the beam on elastic foundation model could only be employed to model one sub-beam. In case of a general bi-layer beam-type interface fracture specimen, a sub-layer (or sub-laminate in composite laminates) model (Armanios et al., 1986; Wang and Qiao, 2004a) is more suitable. In this type of model, each layer of the virgin beam near the crack tip was modeled as a single sub-beam, instead of only considering the whole uncracked portion as a composite beam in the conventional way (Schapery and Davidson, 1990; Suo and Hutchinson, 1990). Thus, each layer has individual rotation, and the cross-section at the joint does not remain a plane as assumed in the composite beam model. In this regard, the joint (crack tip) is rotationally flexible and can be determined by the beam analysis (Wang and Qiao, 2004a). However, the assumption that the interface stresses have no effect on the deformations of sub-beams was used (Wang and Qiao, 2004a), which leads to a "semi-rigid joint" scenario at the crack tip of the two sub-layers and the underestimated local deformation as compared to numerical finite element solution (Li et al., 2004). A need exists to modify the semi-rigid joint model so that a better estimation of local deformation at the crack tip can be obtained and the ERR and mode mixity of the beam-type fracture specimens can be thus better estimated.

To this end, an improved sub-layer beam model is first presented in this study. In contrast to the aforementioned "semi-rigid joint" sub-layer model (Wang and Qiao, 2004a), the present method employs a "flexible joint" model, in which the deformations at the crack tip due to the interface stresses are considered by introducing two interface compliances. The concept of crack tip element proposed by Davidson et al. (1995) is herein adapted for the convenience of analysis, and a closed-form solution of crack tip deformation is correspondingly obtained. The new crack deformation solution is then used to derive the improved equations of ERR and mode mixity for

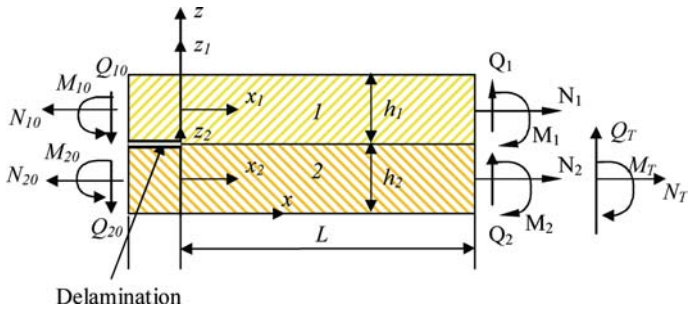

Figure 1. Interface fracture in a bi-layer structure.

commonly used beam-type fracture specimens. Numerical analysis and comparisons are also conducted to verify and illustrate the improved solutions.

2. Bi-layer beam model with flexible joint

Consider a split bi-layered beam under general loading of Figure 1, where a crack lies along the straight interface of the top beam "1" and bottom beam "2" with thickness of h_1 and h_2, respectively. Two beams are made of homogenous, orthotropic materials, with the orthotropy axes along the coordinate system. The length of the uncracked region L is relatively large compared to the thickness of the whole beam h_1+h_2 so that the effect of boundary conditions of the virgin part is negligible. This configuration essentially represents a crack tip element, a small element of a split beam where the cracked and uncracked portions are joining, on which the generic loads are applied, as already determined by a global beam analysis. It is assumed that the length of cracked and uncracked parts of the beam is relatively large compared to the bi-layer beam thickness. Therefore, a beam theory can be used to model the behavior of the top and bottom layers.

Considering a typical infinitesimal isolated body of bi-layer beam system (Figure 2), the following equilibrium equations are established:

$$\begin{aligned}
&\frac{dN_1(x)}{dx}=b\tau(x), \quad \frac{dN_2(x)}{dx}=-b\tau(x),\\
&\frac{dQ_1(x)}{dx}=b\sigma(x), \quad \frac{dQ_2(x)}{dx}=-b\sigma(x),\\
&\frac{dM_1(x)}{dx}=Q_1(x)-\frac{h_1}{2}b\tau(x), \frac{dM_2(x)}{dx}=Q_2(x)-\frac{h_2}{2}b\tau(x),
\end{aligned} \tag{1}$$

where $N_1(x)$ and $N_2(x)$, $Q_1(x)$ and $Q_2(x)$, and $M_1(x)$ and $M_2(x)$ are the axial forces, transverse shear forces, and bending moments in layers 1 and 2, respectively, b is the width of the beam, h_1 and h_2 are the thickness of layers 1 and 2, respectively, $\sigma(x)$ and $\tau(x)$ are the interface normal (peel) and shear stresses, respectively.

By making use of the constitutive equations of the individual layers, we can relate the stress resultants and displacements of plates as

$$N_i=A_i\frac{du_i}{dx}, \quad M_i=D_i\frac{d\phi_i}{dx}, \quad Q_i=B_i\left(\phi_i+\frac{dw_i}{dx}\right), \tag{2}$$

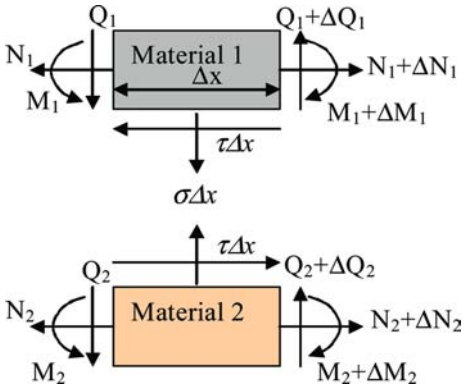

Figure 2. Free body diagram of sub-layers.

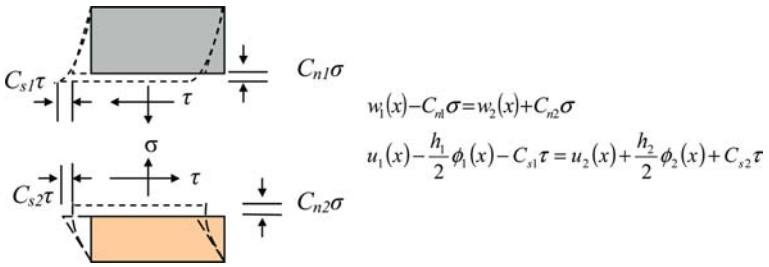

Figure 3. Displacement continuity conditions along the interface of sub-layers.

where A_i, B_i, and $D_i (i = 1, 2)$ are the axial, shear and bending stiffness coefficients of layer i, respectively, and they are expressed as

$$A_i = E_{11}^{(i)} b h_i, \quad B_i = \frac{5}{6} G_{13}^{(i)} b h_i, \quad D_i = E_{11}^{(i)} \frac{b h_i^3}{12},$$

where $E_{11}^{(i)}$ and $G_{13}^{(i)}$ $(i = 1, 2)$ are the longitudinal Young's modulus and transverse shear modulus of layer i, respectively.

The overall equilibrium requires (Figure 1)

$$\begin{aligned} &N_1 + N_2 = N_{10} + N_{20} = N_T, \quad Q_1 + Q_2 = Q_{10} + Q_{20} = Q_T, \\ &M_1 + M_2 + N_1 \frac{h_1 + h_2}{2} = M_{10} + M_{20} + N_{10} \frac{h_1 + h_2}{2} + Q_T x = M_T \end{aligned} \tag{3}$$

where N_{i0}, Q_{i0} and M_{i0} $(i = 1, 2)$ are the external forces in layers 1 and 2, respectively, N_T, Q_T and M_T are the resulting forces expressed by the right equality in the above equations.

To overcome the drawback of the semi-rigid joint condition used in the existing bi-layer beam model (Wang and Qiao, 2004a) aforementioned, the continuity conditions of deformation along the interface (Figure 3) are therefore modified by the new terms of compliance contributions from the interface stresses and become

$$w_1(x) - C_{n1}\sigma = w_2(x) + C_{n2}\sigma, \tag{4}$$

$$u_1(x) - \frac{h_1}{2}\phi_1(x) - C_{s1}\tau = u_2(x) + \frac{h_2}{2}\phi_2(x) + C_{s2}\tau, \tag{5}$$

where C_{ni} and C_{si} are the interface compliance coefficients of the bi-layer beam under peel and shear stresses, to account for the contribution of interface stresses to the displacement components at the interface of two layers. The concept of the interface compliance was first introduced by Suhir (1986) to study the stresses in the bi-metal thermostats. In this way, the existing sub-laminate model (Armanios et al., 1986; Chartterjee and Ramnath, 1988; Zou et al., 2001; Wang and Qiao, 2004a) is a special case of Equations (4) and (5) by assuming that the two interface compliance coefficients are zero, which is equivalent to a semi-rigid joint case (Qiao and Wang, 2005, in press). As recently demonstrated by Wang and Qiao (2004b), a good estimation of these two compliances is given by

$$C_{ni} = \frac{h_i}{10E_{33}^{(i)}}, \quad C_{si} = \frac{h_i}{15G_{13}^{(i)}}. \tag{6}$$

The governing equation of a bi-layer beam system is thus established as

$$\frac{d^6N_1}{dx^6} + a_4\frac{d^4N_1}{dx^4} + a_2\frac{d^2N_1}{dx^2} + a_0N_1 + a_MM_T + a_NN_T = 0, \tag{7}$$

where,

$$\begin{aligned}
a_0 &= -b^2K_nK_s\left(\left(\frac{1}{D_1}+\frac{1}{D_2}\right)\eta + \frac{\xi\,(h_1+h_2)}{2D_2}\right),\\
a_2 &= bK_n\left(bK_s\left(\frac{1}{B_1}+\frac{1}{B_2}\right)\left(\eta+\frac{h_1}{2}\xi\right)+\left(\frac{1}{D_1}+\frac{1}{D_2}\right)\right),\\
a_4 &= -b\left(K_s\left(\frac{\xi h_1}{2}+\eta\right)+K_n\left(\frac{1}{B_1}+\frac{1}{B_2}\right)\right),\\
a_M &= -b^2K_nK_s\left(\left(\frac{1}{D_1}+\frac{1}{D_2}\right)\frac{h_2}{2}+\xi\right)\frac{1}{D_2},\\
a_N &= -b^2K_nK_s\left(\frac{1}{D_1}+\frac{1}{D_2}\right)\frac{1}{A_2},\\
K_s &= \frac{1}{C_{s1}+C_{s2}}, \quad K_n = \frac{1}{C_{n1}+C_{n2}}, \quad \xi = \frac{h_1}{2D_1}-\frac{h_2}{2D_2}, \quad \eta = \frac{1}{A_1}+\frac{1}{A_2}+\frac{(h_1+h_2)\,h_2}{4D_2}.
\end{aligned}$$

It is interesting to point out that the present approach accounting for the effects of interface shear and peel stresses on the deformation of each sub-beam is similar to a beam on elastic foundation model (Kanninen, 1973, 1974; Williams, 1989), in which the additional deformation due to the interface stresses are captured as "elastic foundation effect" with two foundation stiffnesses. In this sense, the present model can be viewed as a generalization of the beam on elastic foundation model.

3. Flexible joint at the crack tip

3.1. Joint deformation

Based on the above established novel bi-layer beam model, the following local deformation at the crack tip can be obtained (Qiao and Wang, 2004) and expressed as

$$\begin{pmatrix} u_1(0) \\ \phi_1(0) \\ w_1(0) \\ u_2(0) \\ \phi_2(0) \\ w_2(0) \end{pmatrix} = \begin{pmatrix} u_{1C}(0) \\ \phi_{1C}(0) \\ w_{1C}(0) \\ u_{2C}(0) \\ \phi_{2C}(0) \\ w_{2C}(0) \end{pmatrix} - \begin{pmatrix} S_{11} & S_{12} & S_{13} \\ S_{21} & S_{22} & S_{23} \\ S_{31} & S_{32} & S_{33} \\ S_{41} & S_{42} & S_{43} \\ S_{51} & S_{52} & S_{53} \\ S_{61} & S_{62} & S_{63} \end{pmatrix} \begin{pmatrix} N \\ M \\ Q \end{pmatrix}, \tag{8}$$

where $\{u_1(0), \phi_1(0), w_1(0), u_2(0), \phi_2(0), w_2(0)\}^{\mathrm{T}}$ represents the displacement components of the respective sub-layers at the crack tip of this study; $\{u_{1C}(0),\ \phi_{1C}(0),\ w_{1C}(0),\ u_{2C}(0),\ \phi_{2C}(0),\ w_{2C}(0)\}^{\mathrm{T}}$ represents the displacement components at the crack tip based on the conventional composite beam model (the rigid joint model); $\{\Delta u_1(0), \Delta\phi_1(0), \Delta w_1(0), \Delta u_2(0), \Delta\phi_2(0), \Delta w_2(0)\}^{\mathrm{T}}$ are the difference between the conventional composite beam model and the present study; $\boldsymbol{S} = \{S_{ij}\}_{6\times 3}$ is a matrix representing the local deformation compliance at the crack tip and given in Appendix A; and $\{N, M, Q\}^{\mathrm{T}}$ is the self-equilibrated loading parameters acting at the crack tip and defined by

$$N = N_{10} - N_{1\mathrm{C}}|_{x=0}\ ,\ M = M_{10} - M_{1\mathrm{C}}|_{x=0}\ ,\ Q = Q_{10} - Q_{1\mathrm{C}}|_{x=0}\ , \tag{9}$$

where,

$$N_{1\mathrm{C}} = \frac{(D_1+D_2)\,h_2 + \xi D_1 D_2 (h_1+h_2)}{2D_2(D_1+D_2)\,\eta + \xi D_1 D_2 (h_1+h_2)} M_T + \frac{2(D_1+D_2)}{C_2\,(2(D_1+D_2)\,\eta + (h_1+h_2)\,D_1\xi)} N_T,$$

$$Q_{1\mathrm{C}} = \left(\frac{\eta}{\xi} + \frac{h_1}{2}\right) \frac{(D_1+D_2)\,h_2 + D_1 D_2 \xi}{2D_2(D_1+D_2)\,\eta + \xi\,(h_1+h_2)} Q_T,\quad M_{1\mathrm{C}} = \frac{\eta}{\xi} N_{1\mathrm{C}} - \frac{1}{\xi}\left(\frac{N_T}{C_2} + \frac{h_2}{2D_2} M_T\right).$$

Equation (8) provides a new and improved continuity condition at the crack tip, and it represents an elastic deformable joint (Figure 4b) and is therefore more realistic than the rigid joint model used commonly in the literature (Figure 4a). Based on Equation (8), the new and improved solution of a cracked bi-layer beam with inclusion of crack tip deformation can be obtained.

Considering the conventional beam-type fracture specimens, such as the double cantilever beam (DCB) and ENF, in which the loads are applied at the end or the mid-span of the specimens, the compliance can be therefore modified based on Equation (8) to account for the crack tip deformation as

$$C = C_C + C_j \tag{10}$$

where C is the total compliance of the specimen, C_C is the compliance of the specimen calculated based on the conventional composite beam model (with a rigid joint at the crack tip). C_j is a new term representing the contribution of the crack tip deformation to the total compliance of the specimen and is given by

$$C_j = -\frac{n}{2P}(\Delta\phi a + \Delta w) \tag{11}$$

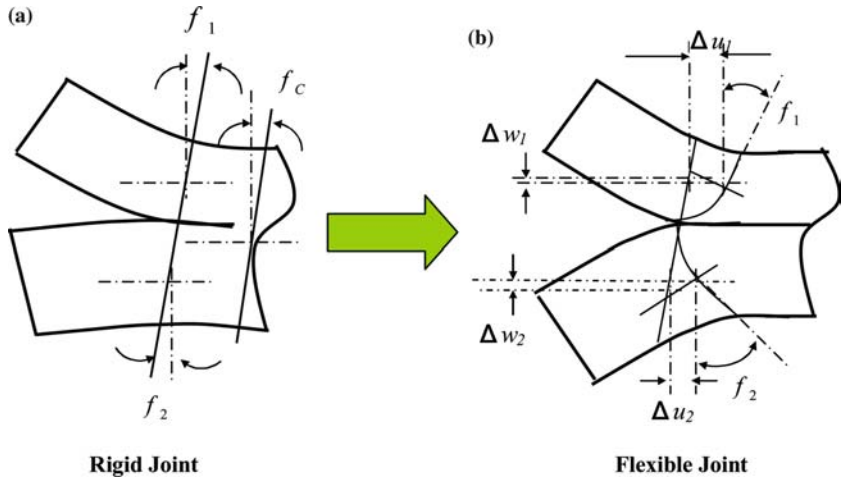

Figure 4. Joint (crack-tip) deformation.

where a is the crack length, and P is the applied load, n is a value corresponding to the load point position, i.e., $n=2$ if the load is applied at the beam end (e.g., DCB) and $n=1$ if at the mid-span of the specimen (e.g., ENF). Consequently, ERR is given as

$$G = G_{\mathrm{C}} + G_j, \quad G_{\mathrm{C}} = \frac{P^2}{2b}\frac{dC_{\mathrm{C}}}{da}, \quad G_j = \frac{P^2}{2b}\frac{dC_j}{da}, \tag{12}$$

where G is the improved ERR of the specimen, G_{C} is the ERR of the rigid joint model by the conventional composite beam theory, and G_j is the additional ERR induced by the crack tip deformation. Again, G_j is the missing term in the conventional rigid joint model and is recovered here to represent the crack tip local deformation effect. With the local deformation considered and captured by a new term C_j in Equations (10) and (12), it is expected that the accuracy in determination of ERR and mode mixity can be improved. Since the local deformation at the crack tip is solved analytically, the improved fracture parameters for the beam-type fracture specimens can be thus determined in the closed-form solutions as illustrated later for several commonly used specimens.

3.2. Numerical verification

To verify the above solutions, the deformations at the joint of a simple split beam configurations shown in Figure 5a is examined by the present method and the finite element analysis (FEA). The specimen is modeled by a commercial finite element package ANSYS as a two-dimensional problem with 8-node structural plane element (PLANE82). The geometries in Figure 5a are chosen as $h_1=h_2=1, L/h_1=1$. Two sets of materials are considered in this study: (a) symmetric DCB specimen: $E_1=E_2=1, \nu_1=\nu_2=0.3$ and; (b) an asymmetric double cantilever beam (ADCB) specimen: $E_2=5E_1=5, \nu_1=\nu_2=0.3$. Figure 5b and c compare the deformed cross-section (the axial displacement) at the crack-tip based on the present solution and FEA at $a/h_1=16$. Excellent agreements between the two methods are achieved, which shows that the significant rotations at the joint are captured by the present

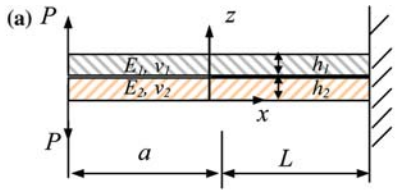

DCB or ADCB specimen

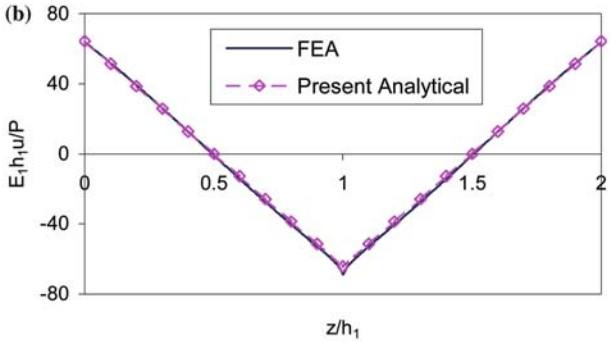

Root rotation of DCB specimen

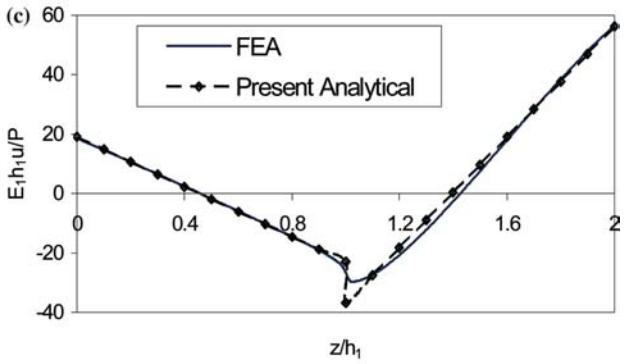

Root rotation of ADCB specimen

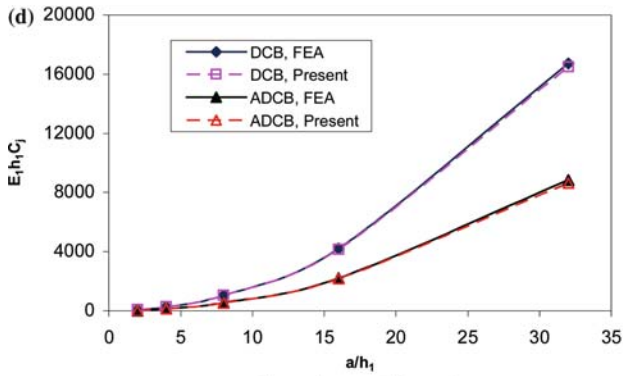

C_j vs. the crack length

Figure 5. Comparisons of joint deformation between the present solution and FEA.

model for both the DCB and ADCB specimens; while in the conventional composite beam model, a zero joint (crack tip) rotation is assumed. In fact, considering Equation (11), the present method provides almost identical solution as that of finite element analysis of C_j for both the DCB and ADCB specimens as demonstrated in Figure 5d.

4. Applications to fracture specimen analyses

The beam-type fracture specimens such as the DCB and ENF specimens have been commonly employed to assess and predict the growth of interface crack of layered structures, such as delamination of composite laminates, debonding of adhesive joints, and decohesion of thin film from substrates. The compliance-based method is one of the most popular techniques to determine the fracture parameters (e.g., ERR and mode mixity) of the beam-type specimens. Varieties of analytical models based on beam theories have been developed for different specimens (Ozil and Carlson, 1999). For the DCB and ENF specimens, very accurate closed-form solutions based on the beam on elastic foundation or higher-order beam theory are available due to the simplicity of the specimen configurations. However, there are no highly accurate analytical solutions for a generic bimaterial interface fracture specimens, such as an asymmetric DCB specimen discussed next. Due to neglecting the local deformation at the crack tip, the existing solutions based on simple beam or Timoshenko's beam theory can only give very approximate predictions when the crack length is comparative to the thickness of the specimen. Meanwhile, unlike the symmetric specimens such as the DCB and ENF, of which the mode mixity is unambiguously defined, there is no accurate way to determine the mode mixity for a generic bimaterial interface specimen. The available solution for the determination of mode mixity (Suo and Hutchinson, 1990; Schapery and Davidson, 1990) was primarily based on simple beam theory, and the transverse shear was not considered. Based on the flexible joint model presented in this study, the compliance-based equations to determine ERR and mode mixity (i.e., for the compliance, ERR and mode mixity) are given in this section, and they account for the local deformation at the crack tip. As illustrated in the following, the resulting solutions of the flexible joint model provide improved accuracy and achieve refined explicitness of fracture parameter equations compared to other available solutions in the literature.

4.1. Double cantilever beam (DCB) specimen

For a DCB (Figure 6) under consideration, three loading parameters of Equation (9) are given by $N=0, M=-Pa, Q=-P$. According to Equation (8) and Appendix A, the deformation at the crack tip is obtained as

$$\Delta w_1 = -\frac{P}{D_1 k_2^2 k_3^2}\left(\left(k_2^2+k_3^2+k_2k_3\right)h^2a+\left(k_2+k_3\right)h^3\right)+\frac{Pa}{B_1},$$

$$\Delta \phi_1 = -\frac{1}{D_1 k_2 k_3}\left(\left(k_2+k_3\right)ha+h^2\right)P. \tag{13}$$

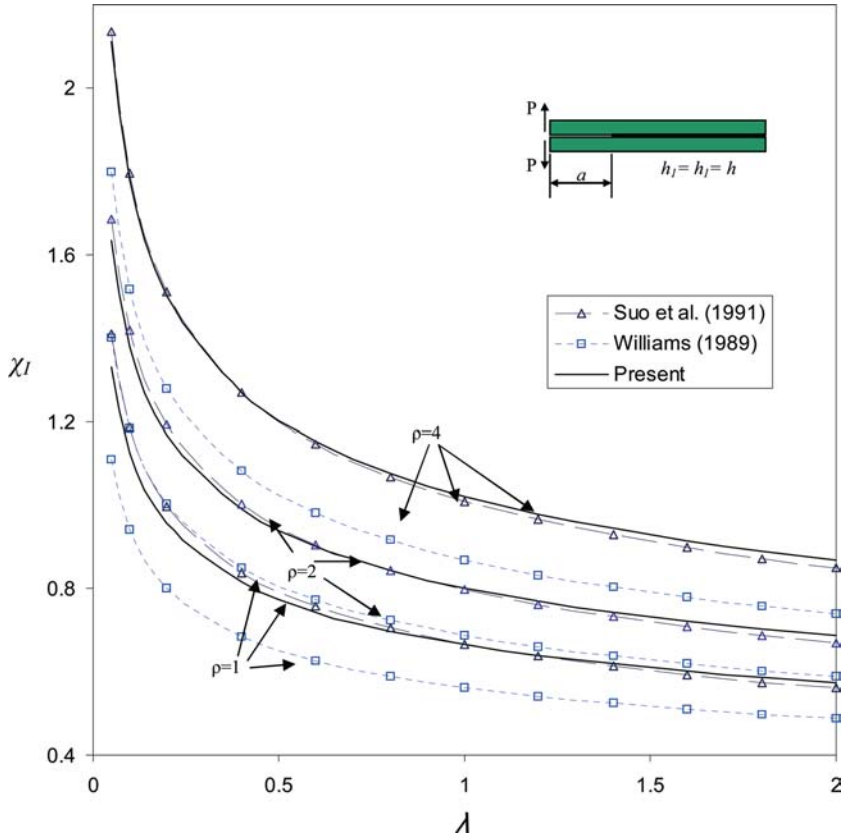

Figure 6. Correction factor for the DCB specimen.

Then, based on Equation (11), the compliance of the DCB specimen at the joint is

$$\frac{1}{2}C_j = -\frac{(\Delta w + \Delta\phi a)}{P} = \frac{k_2+k_3}{D_1 k_2 k_3}ha^2 + \frac{(k_2+k_3)^2}{D_1 k_2^2 k_3^2}h^2 a + \frac{k_2+k_3}{D_1 k_2^2 k_3^2}h^3 - \frac{a}{B_1}. \tag{14}$$

The compliance of the DCB by the conventional composite beam (the rigid joint) model is simply expressed as

$$\frac{1}{2}C_C = \frac{a^3}{3D_1} + \frac{a}{B_1}. \tag{15}$$

Therefore, the improved compliance for the DCB specimen is

$$C = C_C + C_j = \frac{2}{3D_1}a^3 + 2\frac{k_2+k_3}{D_1 k_2 k_3}ha^2 + 2\frac{(k_2+k_3)^2}{D_1 k_2^2 k_3^2}h^2 a + 2\frac{k_2+k_3}{D_1 k_2^2 k_3^2}h^3. \tag{16}$$

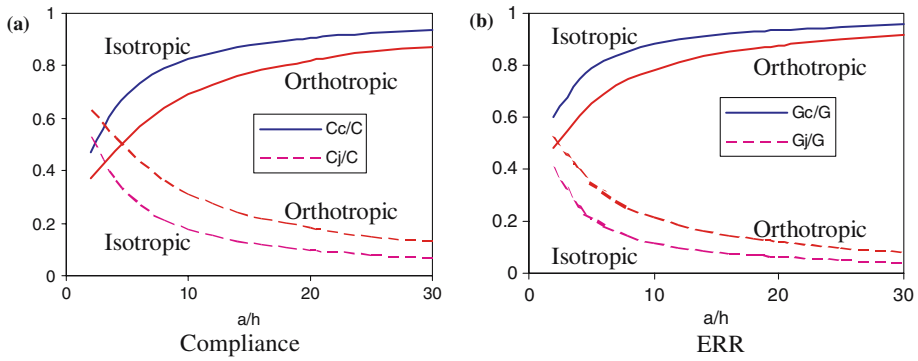

Figure 7. Effect of crack-tip deformation on compliance and ERR of DCB specimen.

Consequently, the ERRs of the DCB specimen are obtained as

$$G_C = \frac{12P^2a^2}{b^2E_{11}h^3} + \frac{P^2}{bB_1},$$

$$G_j = \frac{12P^2}{b^2E_{11}h^3}\left(\frac{2(k_2+k_3)}{k_2k_3}ha + \frac{(k_2+k_3)^2}{k_2^2k_3^2}h^2\right) - \frac{P^2}{bB_1}, \tag{17}$$

$$G = \frac{P^2}{2b}\frac{dC}{da} = \frac{12P^2a^2}{b^2E_{11}h^3}\left(1+\chi_I\left(\frac{h}{a}\right)\right)^2, \tag{18}$$

where $\chi_I = (k_1+k_2)/k_1k_2$. Note that Equation (18) has the same form as Williams's solution (1989) based on a beam on elastic foundation and Suo et al.'s solution (1991) based on the numerical analysis, with the only difference in the expression of χ_I which was called the correction factor by Williams (1989). The expression of the correction factor (χ_I) by Williams (1989) is given as

$$\chi_I = \sqrt{\frac{1}{18K}\left(\frac{a_{66}}{a_{11}}\right)}\left[3-2\left(\frac{\Gamma}{1+\Gamma}\right)^2\right]^{1/2}, \quad \Gamma = \frac{1}{K}\frac{a_{66}}{\sqrt{a_{11}a_{22}}}, \tag{19}$$

where $a_{ii}\,(i=1,2,6)$ are the compliance coefficients of orthotropic materials, and K is the shear correction factor.

A comparison of the values of χ_I by the above three methods (i.e., the present model, Williams's solution (1989) based on a beam on elastic foundation, and Suo et al.'s solution (1991) based on the numerical analysis) is presented in Figure 6. It can be observed that the present closed-form solution is very close to the numerical solution of Suo et al. (1991) with an error less than 1%; while the solution given by Williams (1989) underestimates the correction factor χ_I.

In Equations (16) and (18), the new terms C_j and G_j represent the contribution of local deformation at the crack tip, in addition to the conventional solutions of compliance C_C and ERR G_C based on the rigid joint model in which the two sub-beams in the cracked portion of the specimen are assumed cantilevered at the crack tip. As illustrated in Figure 7, C_j and G_j are quite significant when the crack length is short enough compared to the thickness of the specimen. For example, the crack tip deformation contributes 17% and 30% to the total compliance, 12% and 22% to the total ERR

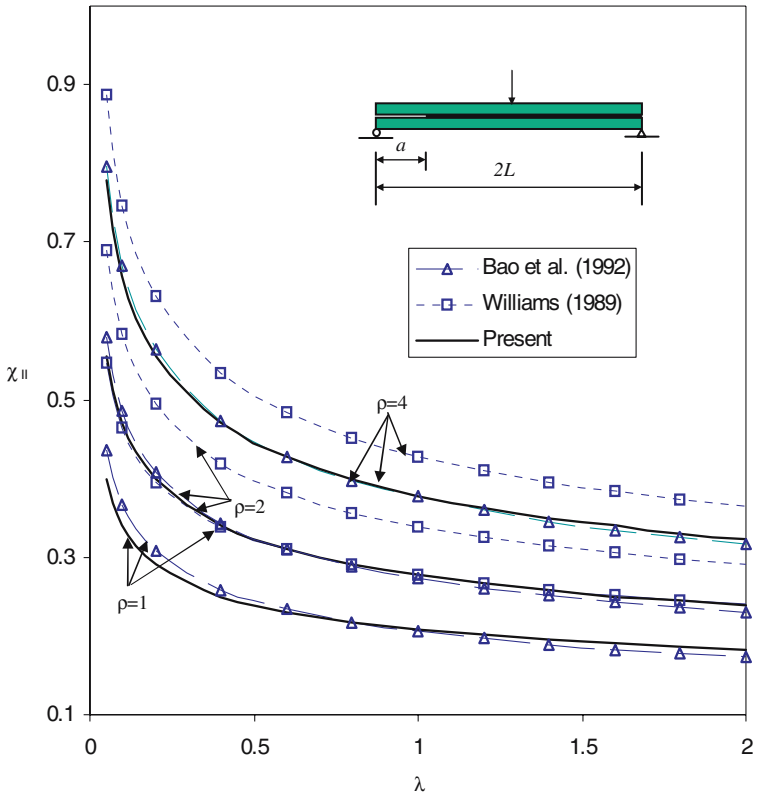

Figure 8. Correction factor for the ENF specimen.

for isotropic and orthotropic materials, respectively, when $a = 10h$. In Figure 7, the isotropic material properties are determined by $\lambda = 1$ and $\rho = 1$; while the orthotropic material properties are defined by $\lambda = 0.2$ and $\rho = 2$. λ and ρ are the two nondimensional parameters defined by Suo et al. (1991) as $\lambda = \frac{E_{33}}{E_{11}}$, $\rho = \frac{\sqrt{E_{11}E_{33}}}{2G_{13}} - \sqrt{\nu_{13}\nu_{31}}$.

4.2. End-notched-flexural (ENF) specimen

The ENF specimen is a standard specimen commonly used in measuring the mode-II fracture toughness of materials. Similar to the procedures for the DCB specimen, the local deformation at the crack tip for the ENF specimen (Figure 8) is obtained as

$$\Delta\phi_1 = -\frac{3Pah}{16D_1k_1}, \quad \Delta w_1 = -\frac{3Pah^2}{16D_1k_1^2}. \tag{20}$$

Then the improved expression of compliance and ERR accounting for the crack tip deformation can be presented as

$$C_j = -\frac{1}{2P}(\Delta\phi_1 a + \Delta w_1) = \frac{3}{32D_1}\left(\frac{a^2h}{k_1} + \frac{ah^2}{k_1^2}\right), C_C = \frac{L}{4B_1} + \frac{L^3}{48D_1} + \frac{a^3}{32D_1}, \tag{21}$$

$$C = \frac{L}{4B_1} + \frac{L^3}{48D_1} + \frac{1}{32D_1}\left(a^3 + \frac{3a^2h}{k_1} + \frac{3ah^2}{k_1^2}\right), \tag{22}$$

$$G_C = \frac{9P^2a^2}{16b^2E_{11}h^3}, \quad G_j = \frac{9P^2a^2}{16b^2E_{11}h^3}\left(\frac{2ah}{k_1} + \frac{h^2}{k_1^2}\right), \tag{23}$$

$$G = \frac{9P^2a^2}{16b^2E_{11}h^3}\left(1 + \chi_{II}\frac{h}{a}\right)^2, \tag{24}$$

where $\chi_{II} = 1/k_1$. Similar expressions of the ERR were obtained by Williams (1989) based on the beam on elastic foundation and Bao et al. (1992) based on the numerical analysis. However, the different formulas were presented in their study to calculate the correction factor χ_{II}. A revised expression of χ_{II} obtained by Wang and Williams (1992) were given as

$$\chi_{II} = \sqrt{\frac{1}{63}\left(\frac{a_{66}}{a_{11}}\right)}\left[3 - 2\left(\frac{\Gamma}{1+\Gamma}\right)^2\right]^{1/2}, \quad \Gamma = \frac{1}{K}\frac{a_{66}}{\sqrt{a_{11}a_{22}}}, \tag{25}$$

where $a_{ii}(i = 1, 2, 6)$ are the compliance coefficients of orthotropic materials, and K is the shear correction factor.

Equation (25) shows that $\chi_{II} = 0.42\chi_I$. A comparison of χ_{II} based on Wang and Williams's approach (1989) (Equation (25)), Bao et al.'s numerial result (1992) and the present solution is given in Figure 8. It can be observed that the present closed-form solution is very close to the numerical solution of Bao et al. (1992) with an error less than 1%; while the solution given by Williams (1989) predicts a little larger value of χ_{II}. As indicated in Equation (22), the influence of crack tip deformation on the total compliance of the ENF specimen is not significant when the crack length is large; while the contribution of crack tip deformation to the total ERR is quite pronounced (see Equation (24)). By observing Figures 6 and 8, it indicates the correction factor (χ_I) for the DCB specimen is about three times of χ_{II} for the ENF specimen.

4.3. Asymmetric DCB specimen

An ADCB specimen (Figure 9) is a simple but effective specimen for measurement of polymer/polymer and polymer/non-polymer bimaterial interface fracture toughness. It has a similar loading configuration as the DCB specimen but with different materials and thickness for each sub-beam. Accordingly, the expressions of compliance and ERR can be solved as

$$C_C = \frac{a^3}{3}\left(\frac{1}{D_1} + \frac{1}{D_2}\right) + a\left(\frac{1}{B_1} + \frac{1}{B_2}\right), \tag{26}$$

$$C_j = (S_{22} - S_{52})a^2 + (S_{32} - S_{62} + S_{23} - S_{53})a + S_{33} - S_{63}, \tag{27}$$

$$C = \frac{a^3}{3}\left(\frac{1}{D_1} + \frac{1}{D_2}\right) + a\left(\frac{1}{B_1} + \frac{1}{B_2}\right) + (S_{22} - S_{52})a^2 + (S_{32} - S_{62} + S_{23} - S_{53})a + S_{33} - S_{63}, \tag{28}$$

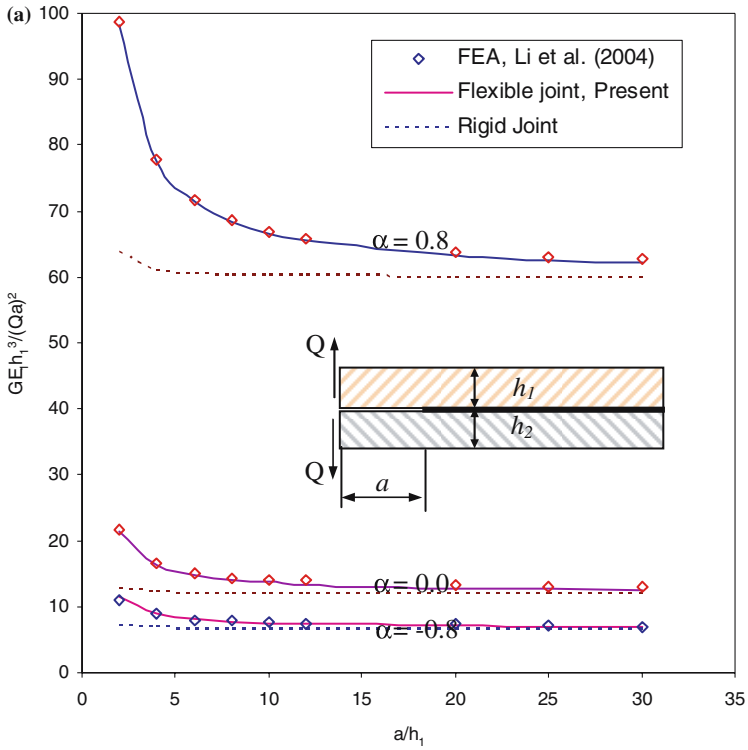

Energy release rate

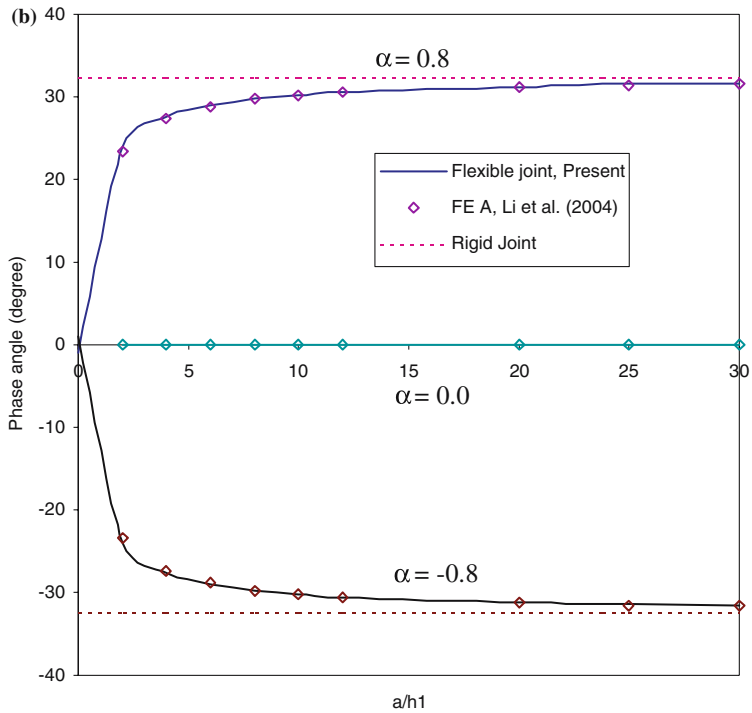

Phase angle

Figure 9. Comparison of fracture parameters for the ADCB specimen ($h_1 = h_2$).

$$G_C = \frac{P^2 a^2}{2b}\left(\frac{1}{D_1}+\frac{1}{D_2}\right)+\frac{P^2}{2b}\left(\frac{1}{B_1}+\frac{1}{B_2}\right),$$
$$G_j = \frac{P^2}{2b}\left(2\left(S_{22}-S_{52}\right)a+S_{32}-S_{62}+S_{23}-S_{53}\right), \tag{29}$$

$$G = \frac{P^2}{2b}\left(\left(\left(\frac{1}{D_1}+\frac{1}{D_2}\right)a^2+2\left(S_{22}-S_{52}\right)a + \left(\frac{1}{B_1}+\frac{1}{B_2}+\left(S_{32}-S_{62}\right)+\left(S_{23}-S_{53}\right)\right)\right)\right). \tag{30}$$

To obtain the mode mixity, the complex stress intensity factor is defined by using the combination $Kh_1^{i\varepsilon}$ as suggested by Rice (1988) as

$$Kh_1^{i\varepsilon} = K_I + iK_{II} = |K|e^{i\psi}. \tag{31}$$

Then the individual stress intensity factors are given based on *J*-integral approach of Qiao and Wang (2004) as

$$K_I = \frac{p}{\sqrt{2}}\left(\sqrt{C_M}a\,\sin\left(\omega+\gamma_1\right)+\sqrt{C_Q}\sin\left(\omega+\gamma_2\right)\right), \tag{32}$$

$$K_{II} = \frac{p}{\sqrt{2}}\left(-\sqrt{C_M}a\,\cos\left(\omega+\gamma_1\right)-\sqrt{C_Q}\cos\left(\omega+\gamma_2\right)\right). \tag{33}$$

The phase angle ψ is therefore obtained as

$$\psi = \tan^{-1}\left(\frac{-\sqrt{C_M}a\,\cos\left(\omega+\gamma_1\right)-\sqrt{C_Q}\cos\left(\omega+\gamma_2\right)}{\sqrt{C_M}a\,\sin\left(\omega+\gamma_1\right)+\sqrt{C_Q}\sin\left(\omega+\gamma_2\right)}\right). \tag{34}$$

The related coefficients in Equations (32) and (34) are defined by Qiao and Wang (2004) and given as follows:

$$C_N = \frac{1}{C_1}+\frac{1}{C_2}+\frac{(h_1+h_2)^2}{4D_2},\quad C_Q = \frac{1}{B_1}+\frac{1}{B_2}+S_{23}-S_{53},$$
$$C_{NQ} = S_{21}-S_{51},\quad C_{MQ} = S_{22}-S_{52},\quad C_{MN} = \frac{h_1+h_2}{D_2},$$
$$\sin\left(\gamma_1\right) = \frac{C_{MN}}{2\sqrt{C_M C_N}},\quad \sin\left(\gamma_2\right) = \frac{C_{NQ}}{2\sqrt{C_N C_Q}}.$$

As a verification of the present solution, an ADCB specimen is studied, and then the proposed analytical solution is compared with the finite element results of Li et al. (2004). A value of 0.3 is chosen for the Poisson's ratio of both substrate materials, and an excellent agreement (with a maximum error of 1%) is achieved when compared to the FEA results for both the ERR and phase angle (Figure 9). Note that the high accuracy of the present solution is valid for the entire material mismatch ranging from $\alpha = -0.8$ to 0.8. To show the necessity of including crack tip deformation in the formulation, the ERR and phase angle are also calculated by the conventional rigid joint model and presented in Figure 9. It is not surprising to observe that the large discrepancy exists between the conventional rigid joint model and either the current flexible joint model or finite element analysis when the crack length is small or comparable to the thickness of the specimen. Meanwhile, the classical solution

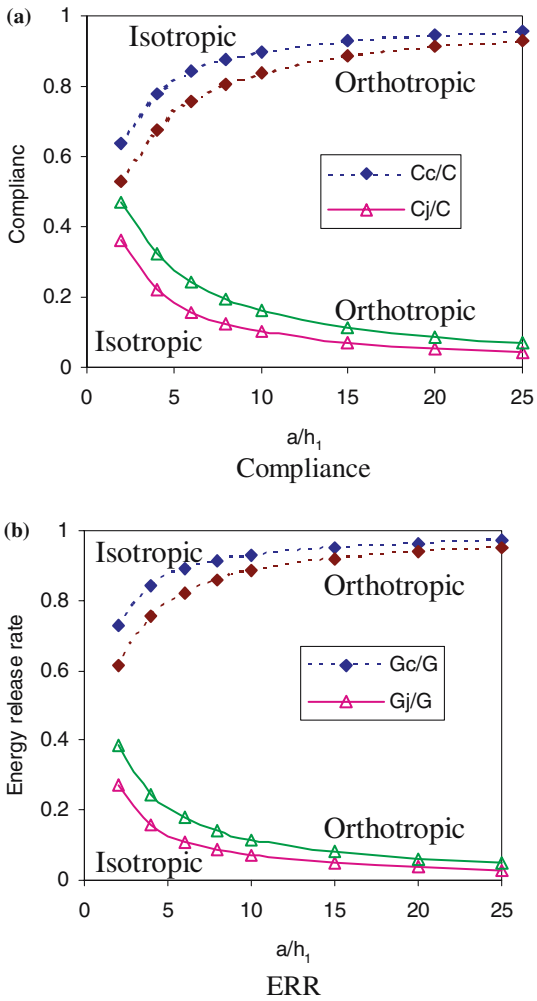

Figure 10. Effect of crack-tip deformation on compliance and ERR of ADCB specimen.

of phase angle (Suo and Hutchinson, 1990; Schapery and Davidson, 1990) could only produce a constant phase angle for this specimen; however, the phase angle in fact varies with the length of the crack as revealed by the finite element analysis. The reason for this shortcoming of the classical solution is that the transverse shear force is ignored in the model. Since the transverse shear force is not considered in the classical solution, there are some misunderstandings in the available literature, such as Williams (1988) and Nilsson et al. (2001) in which both assumed that the transverse shear only produces the mode-I ERR. Equations (32)–(34) show that the transverse shear is contributive to both the mode-I and mode-II fracture, and this feature is verified by the excellent agreement with finite element analysis. Ignoring the effect of transverse shear leads to overestimation of loading phase angle as indicated in Figure 9, especially when the crack length is small. By accounting for the local deformation at the crack tip, the transverse shear effect on the phase angle is fully considered in the present model. The significant effect of local deformation on the compliance and ERR can be further illustrated by Figure 10. It can be observed

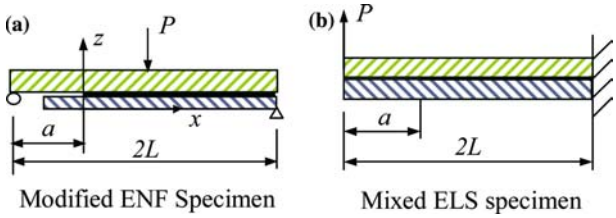

Figure 11. Mixed-mode fracture specimens.

that the crack-tip deformation contributes about 10% and 16% to the total compliance, and around 7% and 12% to the total ERR for isotropic and orthotropic materials, respectively, when $a = 10h_1$. In Figure 10, $h_1 = 2h_2$, $\lambda = 1$ and $\rho = 1$ are chosen for isotropic material, $\lambda = 0.2$ and $\rho = 2$ for orthotropic material. The close agreement with the finite element analysis solution shows that the current solution improves the prediction accuracy of ERR and mode mixity for the ADCB specimen. It should be pointed out that the fracture experiment using the ADCB specimen is an inherently non-linear test (Sundararaman and Davidson, 1997). While both the finite element solution of Li et al. (2004) and the present analytical solution are based on the assumption of linear elastic deformation. Cautions should be taken when applying the present solution in the experimental data analysis and reduction.

4.4. Modified end notched flexure specimen

Two mixed mode specimens presented in Figure 11 have the same loading configuration at the crack tip, except that the load in the mixed mode End-Loaded Split (ELS) specimen is two times as the modified ENF specimen. Therefore, a similar solution of crack tip deformation can be obtained based on Equation (8). For the sake of brevity, only the solution of modified ENF specimen is presented below.

Based on the present flexible joint model, the related equations for the modified ENF specimen are given as

$$C_{\mathrm{C}} = \frac{2L + a\,(R_1 - 1)}{4B_T} + \frac{2L^3 + a^3\,(\mathrm{R}_2 - 1)}{12D_T}, \tag{35}$$

$$C_j = \frac{1}{4}\left((S_{21}A_n + S_{22}A_m)\,a^2 + \left(S_{31}A_n + S_{32}A_m + S_{23}A_q\right)a + S_{33}A_q\right), \tag{36}$$

$$C = \frac{2L + a\,(R_1 - 1)}{4B_T} + \frac{2L^3 + a^3\,(R_2 - 1)}{12D_T} + \frac{1}{4}\left((S_{21}A_n + S_{22}A_m)\,a^2 + \left(S_{31}A_n + S_{32}A_m + S_{23}A_q\right)a + S_{33}A_q\right), \tag{37}$$

$$G_{\mathrm{C}} = \frac{P^2}{2b}\left(\frac{R_2 - 1}{4D_T}a^2 + \frac{R_1 - 1}{4B_T}\right), \tag{38}$$

$$G_j = \frac{P^2}{4b}\left((S_{21}A_n + S_{22}A_m)\,a + \frac{1}{2}\left(S_{31}A_n + S_{32}A_m + S_{23}A_q\right)\right),$$

$$G = \frac{P^2}{2b}\left(\frac{R_2 - 1}{4D_T}a^2 + \frac{R_1 - 1}{4B_T} + (S_{21}A_n + S_{22}A_m)\,\frac{a}{2} + \frac{1}{4}\left(S_{31}A_n + S_{32}A_m + S_{23}A_q\right)\right), \tag{39}$$

where $R_1 = B_T/B_1$, $R_2 = D_T/D_1$; B_T and D_T are the shear and bending stiffness of the virgin portion of the specimen, respectively. Other coefficients are given as

$$A_n = \frac{a_M}{a_0}, \quad A_m = 1 + \frac{a_M}{a_0}\frac{\eta}{\xi} + \frac{h_2}{2D_2\xi}, \quad A_q = 1 + \frac{a_M}{a_0}\left(\frac{h_1}{2} + \frac{\eta}{\xi}\right) + \frac{h_2}{2D_2\xi}.$$

The stress intensity factors are given by

$$K_I = \frac{p}{\sqrt{2}}\left(\sqrt{C_N}A_n a\cos(\omega) + \sqrt{C_M}A_m a\sin(\omega+\gamma_1) + \sqrt{C_Q}A_q\sin(\omega+\gamma_2)\right), \quad (40)$$

$$K_{II} = \frac{p}{\sqrt{2}}\left(\sqrt{C_N}A_n a\sin(\omega) - \sqrt{C_M}A_m a\cos(\omega+\gamma_1) - \sqrt{C_Q}A_q\cos(\omega+\gamma_2)\right). \quad (41)$$

The phase angle ψ is then given by

$$\psi = \tan^{-1}\left(\frac{\sqrt{C_N}A_n a\sin(\omega) - \sqrt{C_M}A_m a\cos(\omega+\gamma_1) - \sqrt{C_Q}A_q\cos(\omega+\gamma_2)}{\sqrt{C_N}A_n a\cos(\omega) + \sqrt{C_M}A_m a\sin(\omega+\gamma_1) + \sqrt{C_Q}A_q\sin(\omega+\gamma_2)}\right). \quad (42)$$

To validate the present solution, we analyze a modified ENF specimen studied in detail by Davidson and Sundararaman (1996) (referred as the single leg bending (SLB) test in their study). In their work, the ERR and mode mixity of the SLB test were obtained through two approaches: rigid joint model (crack tip element) analysis and finite element (FE) analysis. Three types of specimens with bimaterial interfaces were considered: homogeneous, aluminum/niobium, and glass/epoxy, which essentially "spanned" the range of the material property mismatch ratios one would expect to encounter in practical applications. Details of material properties and specimen geometry were given in their paper (Davidson and Sundararaman, 1996) and therefore omitted here for brevity. The ERR and mode mixity are calculated using Equations (39) and (42), and they are compared with the rigid joint model and FE analyses in Davidson and Sundararaman (1996) (Figure 12). The ERR values in Figure 12 are normalized by the FE analysis results, which are regarded as the accurate ones in this study, and they are in a function of the thickness ratio of upper (top) and lower (bottom) plates. As observed in Figure 12, the rigid joint analysis provides very approximate prediction, underestimating the ERR up to 13.7% for the glass/epoxy interface specimen when compared to the FE analysis. An excellent agreement with finite element analysis is achieved by the present study of flexible joint model, in which the error is within 0.3%. Therefore, by considering the effect of local deformation at the crack tip, the present prediction of the ERR using Equation (39) has significantly improved the accuracy when compared to the conventional approach based on the rigid joint model. It further indicates that the local deformation effect is significant in the interface fracture analysis, especially for the specimens with low transverse shear modulus and moderate thickness.

The comparisons of the phase angles ψ of the SLB test among the rigid joint model, the present study of flexible joint, and FE analysis are presented in Figure 13. It is observed that compared to the rigid joint model analysis, the phase angle by the present study (Equation (42)) is more close to the FE analysis data. Similar to the ADCB specimen, the rigid joint model seems to overestimate the phase angle of the mode mix (if the sign of the phase angle is ignored) due to ignoring the transverse shear, although the difference from the FE analysis is not significant. Both of these

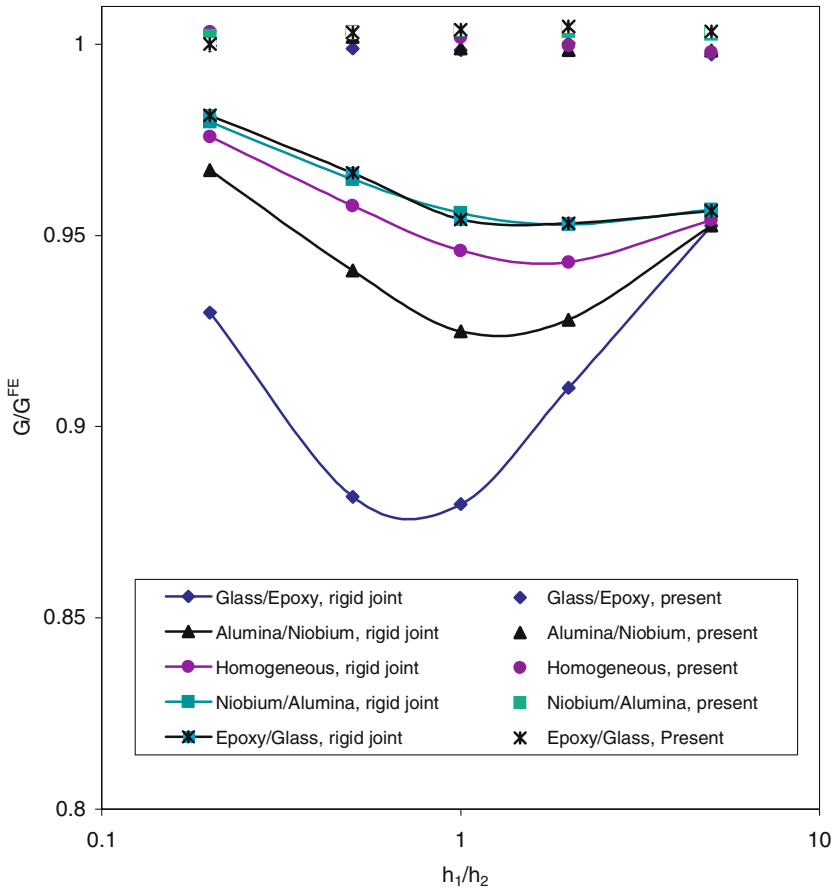

Figure 12. Comparison of energy release rate of SLB specimen at crack-tip for $a/(h_1+h_2)=8.33$ and $a/L=0.5$.

two specimens show that the transverse shear deformation reduces the phase angle, and the accuracy of the phase angle provided by the present formula Equation (42) is improved. The effect of transverse shear on the phase angle is further illustrated in Figure 14 where the phase angle of the SLB specimen is not a constant as assumed in the conventional rigid joint model (Davidson and Sundararaman, 1996). As a matter of fact, the phase angle of SLB specimen varies with the crack length as reflected in Equation (42), in which the phase angle ψ is expressed as a function of crack length a. Figure 14 shows that the existing classical equation tends to overestimate the phase angle considerably when the crack length is small, and a fixed mode mixity using the SLB specimen can only be achieved approximately with a very slender geometry.

To evaluate the accuracy of the present solution for the different thickness ratios, we further examine a homogeneous modified ENF specimen for which a highly accurate solution of the ERR was obtained by Bao et al. (1992) through a finite element analysis and data fitting approach. The ERRs by the present solution are normalized by the conventional rigid joint solution (Williams, 1988), and compared with the numerical results by Bao et al. (1992) (Figure 15). It has been shown in Figure 15 that for the thickness ratio range of 0.2–0.8, the present analytical solution

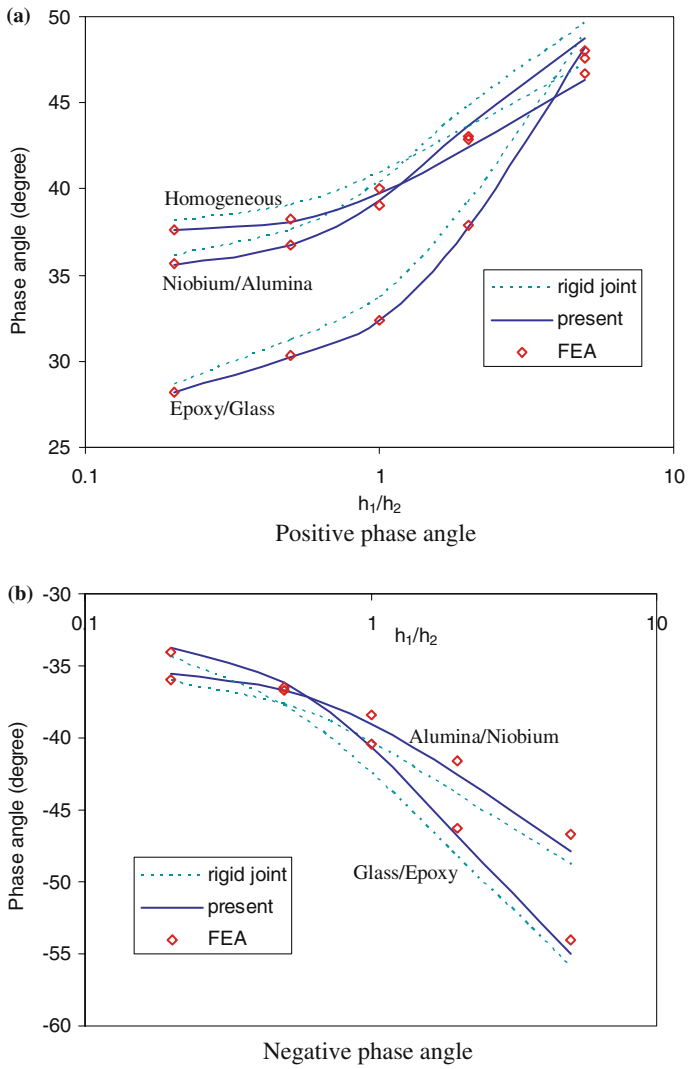

Figure 13. Comparison of phase angles of SLB specimen.

predicts very close values of the ERR to Bao et al. (1992)'s results; the difference between these two methods is less than 1%. Figure 15 also shows clearly the significance of local deformation in the calculation of ERR; even when the crack length is relatively large, a considerable error still can be introduced by neglecting the crack-tip deformation.

5. Conclusions

In this study, a novel bi-layer beam model is developed to accurately capture the crack-tip deformation, which in turn leads to improved solution of fracture parameters (e.g., compliance, ERR and mode mixity) for beam-type specimens. In this model, a bi-layer beam with interface crack is treated as two separate shear deformable sub-beams bonded perfectly along the interface, and a flexible joint is formed

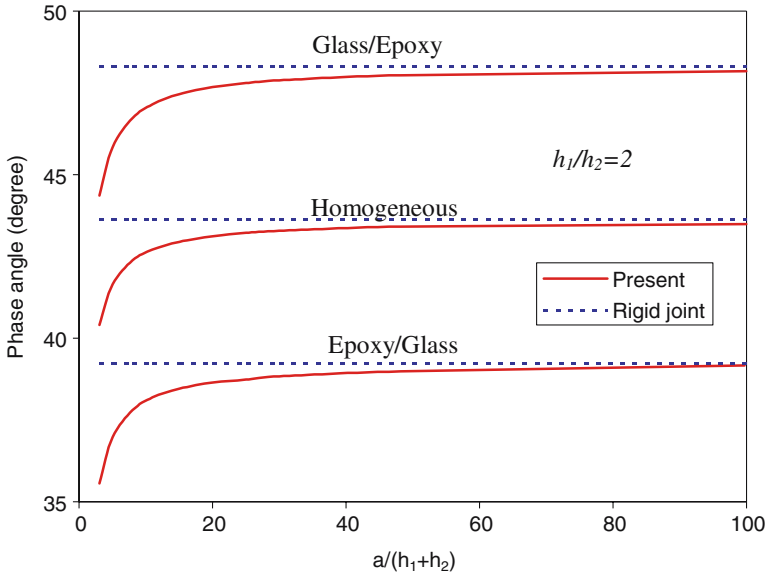

Figure 14. Phase angle vs. crack length for SLB specimen.

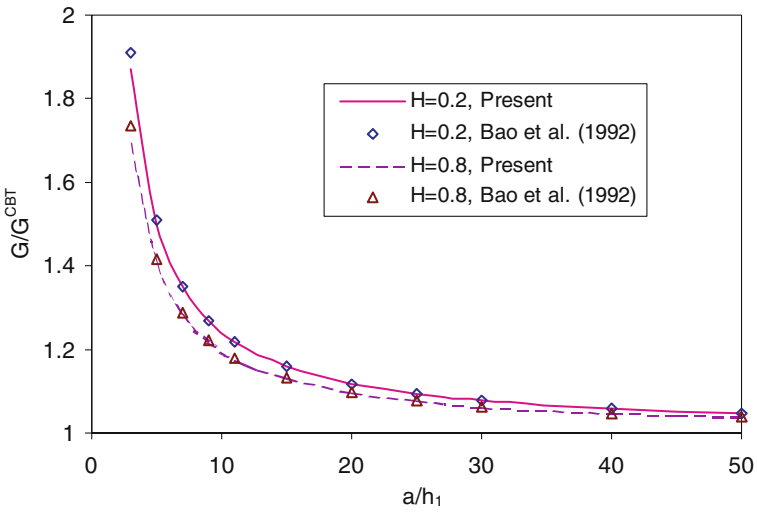

Figure 15. Comparison of ERR of modified ENF specimen $H = h_1/h_2$.

at the crack-tip by employing the concept of two compliance coefficients along the interface to account for the effect of the interface stresses on the deformation of the sub-beams (elastic foundation effect). The crack-tip deformation is obtained in the closed-form and then used to obtain the formulas of compliance and ERR for beam-type fracture specimens. New terms are introduced in the solutions of compliance, ERR and mode mixity, and they are purely due to the crack-tip deformation. These terms are ignored in the conventional rigid joint model solution because of the ignorance of the local deformation at the crack-tip. Using the proposed flexible joint model, the highly accurate equations for determination of ERR and mode mixity of four commonly used fracture specimens, i.e., DCB, ENF, ADCB and SLB

(or modified ENF), are given explicitly. Calculations and comparisons are also made for the specific specimens, of which the accurate solutions are available based on other approaches or numerical analysis. Remarkable agreements with the available solutions and finite element results demonstrate the validity of the present improved analytical solution, as well as the significance of the local deformation at the crack-tip, which cannot be captured by the conventional rigid joint model. As a matter of fact, the error in the available fracture parameter equations commonly used in the data reduction procedure of fracture tests, which are primarily based on the rigid joint model, is mainly caused by the missing terms due to the local deformation at the crack-tip. By adding these missing terms through the present novel flexible joint model, the improved solution provided in this study can produce highly accurate predictions, which can be used to replace the full continuum elasticity analysis such as the finite element analysis.

Acknowledgments

This study was partially supported by the National Science Foundation (CMS-0002829 and EHR-0090472).

References

Armanios, E.A., Rehfield, L. M. and Reddy, A.D. (1986). Design analysis and testing for mixed-mode and mode II interlaminar fracture of composites. In: *Composite Materials: Testing and Design (7th Conference),* ASTM **STP 893**. (Edited by J.M. Whitney.) ASTM, Philadelphia, pp. 232–255.

Bao, G., Ho, S., Suo, Z. and Fan, B. (1992). The role of material orthotropy in fracture specimens for composites. *International Journal of Solids and Structures* **29**, 1105–1116.

Chatterjee, S.N. and Ramnath, V. (1988). Modeling laminate composite structures as assemblage of sublaminates. *International Journal of Solids and Structures* **24**, 439–458.

Corleto, C.R. and Hogan, H.A. (1995). Energy release rates for the ENF specimen using a beam on an elastic foundation. *Journal of Composite Materials* **29**, 1420–1436.

Davidson, B.D., Hu, H. and Schapery, R.A. (1995). An analytical crack-tip element for layered elastic structures. *Journal of Applied Mechanics* **62**, 294–305.

Davidson, B.D. and Sundararaman, V. (1996). A single leg bending test for interfacial fracture toughness determination. *International Journal of Fracture* **78**, 193–210.

Davies, P., Blackman, B.R.K. and Brunner, A.J. (1998). Standard test specimen for delamination resistance of composite materials: current status. *Applied Composite Materials* **5**, 345–364.

Kanninen, H.M. (1973). Augmented double cantilever beam model for studying crack propagation and arrest. *International Journal of Fracture* **9**, 83–92.

Kanninen, H.M. (1974). Dynamic analysis of unstable crack propagation and attest in the DCB specimen. *International Journal of Fracture* **10**, 415–430.

Li, S., Wang, J. and Thouless, M.D. (2004). The effects of shear on delamination in layered materials. *Journal of the Mechanics and Physics of Solids* **52**, 193–214.

Nilsson, K.F., Asp, L.E., Alpman, J.E. and Nystedt, L. (2001). Delamination buckling and growth for delaminations at different depths in a slender composite panel. *International Journal of Solids and Structures* **38**, 3039–3071.

Ozil, F. and Carlsson, L.A. (1999). Beam analysis of angle-ply laminate DCB specimens. *Composites Science and Technology* **59**, 305–315.

Qiao, P., Wang, J., Davalos, J.F. (2003a). Analysis of tapered ENF specimen and characterization of bonded interface fracture under Mode-II loading. *International Journal of Solids and Structures* **40**, 1865–1884.

Qiao, P., Wang, J., and Davalos, J.F. (2003b). Tapered beam on elastic foundation model for compliance rate change of TDCB specimen. *Engineering Fracture Mechanics* **70**(2), 339–353.

Qiao, P. and Wang, J. (2004). Mechanics and fracture of crack-tip deformable bi-material interface. *International Journal of Solids and Structures* **41**(26), 7423–7444.
Qiao, P. and Wang, J. (2005). Novel joint deformation models and their application to delamination fracture analysis. *Composites Science and Technology,* **in press**.
Rice, J.R. (1988). Elastic fracture mechanics concepts for interfacial cracks. *Journal of Applied Mechanics* **55**, 98–103.
Schapery, R.A. and Davidson, B.D. (1990). Prediction of energy release rate for mixed-mode delamination using classical plate theory. *Applied Mechanics Review* **43**, S281–S287.
Shu, D. and Mai, Y. (1993). Buckling of delaminated composites re-examined. *Composites Science and Technology* **47**, 35–41.
Suhir, E. (1986). Stresses in bi-metal thermostats. *Journal of Applied Mechanics* **53**, 657–660.
Sun, C.T. and Pandey, P.K. (1994). Improved method for calculating strain energy release rate based on beam theory. *AIAA Journal* **32**, 184–189.
Sundararaman, V. and Davidson, B.D. (1997). An unsymmetric double cantilever beam test for interfacial fracture toughness determination. *International Journal of Solids and Structures* **34**, 799–817.
Sundararaman, V. and Davidson, B.D. (1998). An unsymmetric end-notched flexure test for interfacial fracture toughness determination. *Engineering Fracture Mechanics* **60**, 361–377.
Suo, Z., Bao, G., Fan, B. and Wang, T.C. (1991). Orthotropy rescaling and implications for fracture in composites. *International Journal of Solids and Structures* **28**, 235–248.
Suo, Z. and Hutchinson, J.W. (1990). Interface crack between two elastic layers. *International Journal of Fracture* **43**, 1–18.
Wang, J. and Qiao, P. (2004a). Interface crack between two shear deformable elastic layers. *Journal of the Mechanics and Physics of Solids* **52**, 891–905.
Wang, J. and Qiao, P. (2004b). Novel beam analysis of end notched flexure specimen for mode-II fracture. *Engineering Fracture Mechanics* **71**, 219–231.
Wang, Y. and Williams, J.G. (1992). Corrections for mode II fracture toughness specimens of composites materials. *Composites Science and Technology* **43**, 251–256.
Williams, J.G. (1988). On the calculation of energy release rate for cracked laminates. *International Journal of Fracture* **36**, 101–119.
Williams, J.G. (1989). End corrections for orthotropic DCB specimens. *Composites Science and Technology* **35**, 367–376.
Zou, Z., Reid, S.R., Soden, P.D. and Li, S. (2001). Mode separation of energy release rate for delamination in composite laminates using sublaminates. *International Journal of Solids and Structures* **38**, 2597–2613.

Appendix A: Compliance matrix of flexible joint in Equation (8)

The governing equation (Equation (7)) derived in Section 2 can be solved through the characteristic equation as

$$x^6 + a_4 x^4 + a_2 x^2 + a_0 = 0. \tag{A1}$$

The roots of the above equation for the given material and geometry parameters can be expressed as: (a) $\pm R_1$, $\pm R_2$ and $\pm R_3$, or (b) $\pm R_1$ and $\pm R_2 \pm i R_3$. Here R_1, R_2 and R_3 are positive real numbers and $i = \sqrt{-1}$.

Case (a). The characteristic equation (Equation (A1)) with roots of $\pm R_1$, $\pm R_2$ and $\pm R_3$

$$S_{1i} = \frac{1}{A_1}\left(\frac{c_{1i}}{R_1} + \frac{c_{2i}}{R_2} + \frac{c_{3i}}{R_3}\right), \quad i = 1, 2, 3,$$
$$S_{2i} = \frac{1}{D_1}\left(\frac{c_{1i}S_1}{R_1} + \frac{c_{2i}S_2}{R_2} + \frac{c_{3i}S_3}{R_3}\right), \quad i = 1, 2, 3$$

$$S_{3i}=\left(\left(\frac{S_1}{D_1R_1^2}+\frac{T_1}{B_1R_1}\right)c_{1i}+\left(\frac{S_2}{D_1R_2^2}+\frac{T_2}{B_1R_2}\right)c_{2i}+\left(\frac{S_3}{D_1R_3^2}+\frac{T_3}{B_1R_3}\right)c_{3i}\right),\quad i=1,2,3,$$

$$S_{4i}=-\frac{1}{A_2}\left(\frac{c_{1i}}{R_1}+\frac{c_{2i}}{R_2}+\frac{c_{3i}}{R_3}\right),\quad i=1,2,3,$$

$$S_{5i}=-\frac{1}{D_2}\left(\frac{c_{1i}S_1}{R_1}+\frac{c_{2i}S_2}{R_2}+\frac{c_{3i}S_3}{R_3}\right)-\frac{h_1+h_2}{2D_2}\left(\frac{c_{1i}}{R_1}+\frac{c_{2i}}{R_2}+\frac{c_{3i}}{R_3}\right),\quad i=1,2,3,$$

$$\begin{aligned}S_{6i}=&-\left(\left(\frac{((h_1+h_2)/2)+S_1}{D_2R_1^2}+\frac{T_1}{B_2R_1}\right)c_{1i}+\left(\frac{((h_1+h_2)/2)+S_2}{D_2R_2^2}+\frac{T_2}{B_2R_2}\right)c_{2i}\right.\\&\left.+\left(\frac{((h_1+h_2)/2)+S_3}{D_2R_3^2}+\frac{T_3}{B_2R_3}\right)c_{3i}\right),\quad i=1,2,3,\end{aligned}\tag{A2}$$

where

$$S_i=-\frac{R_i^2}{\xi}\frac{1}{bK_s}+\frac{\eta}{\xi},\quad T_i=R_i\left(\frac{R_i^2}{\xi}\frac{1}{bK_s}-\frac{\eta}{\xi}-\frac{h_1}{2}\right),\quad i=1,2,3,$$

$$\begin{pmatrix}c_{11}&c_{12}&c_{13}\\c_{21}&c_{22}&c_{23}\\c_{31}&c_{32}&c_{33}\end{pmatrix}=\frac{1}{Y}\begin{pmatrix}S_3T_2-S_2T_3&T_3-T_2&S_2-S_3\\S_1T_3-S_3T_1&T_1-T_3&S_3-S_1\\S_2T_1-S_1T_2&T_2-T_1&S_1-S_2\end{pmatrix},$$

$$Y=S_2T_1-S_3T_1-S_1T_2+S_3T_2+S_1T_3-S_2T_3\tag{A3}$$

Case (b). The characteristic equation (Equation (A1)) with roots of $\pm R_1$ and $\pm R_2\pm iR_3$

$$S_{1i}=\frac{1}{A_1}\left(\frac{c_{1i}}{R_1}+\frac{c_{2i}R_2}{R_2^2+R_3^2}+\frac{c_{3i}R_3}{R_2^2+R_3^2}\right),\quad i=1,2,3,$$

$$S_{2i}=\frac{1}{D_1}\left(\frac{c_{1i}S_1}{R_1}+\frac{c_{2i}\left(R_2S_2+R_3S_3\right)}{R_2^3+R_3^2}+\frac{c_{3i}\left(R_2S_3+R_3S_2\right)}{R_2^3+R_3^2}\right),\quad i=1,2,3,$$

$$\begin{aligned}S_{3i}=&\left(\frac{S_1}{D_1R_1^2}+\frac{T_1}{B_1R_1}\right)c_{1i}+\left(\frac{S_2\left(R_2^2-R_3^2\right)+2R_2R_3S_3}{D_1\left(R_2^2+R_3^2\right)^2}+\frac{T_2R_2+T_3R_3}{B_1\left(R_2^2+R_3^2\right)}\right)c_{2i}\\&+\left(\frac{S_3\left(R_2^2-R_3^2\right)+2R_2R_3S_2}{D_1\left(R_2^2+R_3^2\right)^2}+\frac{T_2R_3+T_3R_2}{B_1\left(R_2^2+R_3^2\right)}\right)c_{3i},\quad i=1,2,3,\end{aligned}$$

$$S_{4i}=-\frac{1}{A_2}\left(\frac{c_{1i}}{R_1}+\frac{c_{2i}R_2}{R_2^2+R_3^2}+\frac{c_{3i}R_3}{R_2^2+R_3^2}\right),\quad i=1,2,3,$$

$$\begin{aligned}S_{5i}=&-\frac{1}{D_2}\left(\frac{c_{1i}\left(((h_1+h_2)/2)+S_1\right)}{R_1}+\frac{c_{2i}\left((((h_1+h_2)/2)+S_2\right)R_2+R_3S_3)}{R_2^3+R_3^2}\right.\\&\left.+\frac{c_{3i}\left((((h_1+h_2)/2)+S_2\right)R_3+R_2S_3)}{R_2^3+R_3^2}\right),\quad i=1,2,3,\end{aligned}$$

$$S_{6i} = -\left(\frac{((h_1+h_2)/2)+S_1}{D_2 R_1^2} + \frac{T_1}{B_2 R_1}\right) c_{1i}$$
$$-\left(\frac{(((h_1+h_2)/2)+S_2)\left(R_2^2-R_3^2\right)+2R_2R_3S_3}{D_2\left(R_2^2+R_3^2\right)^2} - \frac{T_2R_2+T_3R_3}{B_2\left(R_2^2+R_3^2\right)}\right) c_{2i}$$
$$-\left(\frac{S_3\left(R_2^2-R_3^2\right)+2R_2R_3\left(((h_1+h_2)/2)+S_2\right)}{D_2\left(R_2^2+R_3^2\right)^2} - \frac{T_2R_3+T_3R_2}{B_2\left(R_2^2+R_3^2\right)}\right) c_{3i}, \quad i=1,2,3, \tag{A4}$$

where

$$S_1 = -\frac{R_1^2}{\xi b K_s} + \frac{\eta}{\xi}, \quad S_2 = -\frac{R_2^2-R_3^2}{\xi b K_s} + \frac{\eta}{\xi}, \quad S_3 = \frac{2R_2R_3}{\xi b K_s},$$
$$T_i = -R_1S_1 - \frac{h_1}{2}R_1, \quad T_2 = -R_2S_2 + S_3R_3 - \frac{h_1}{2}R_2, \quad T_3 = -R_2S_3 + S_2R_3 - \frac{h_1}{2}R_3,$$
$$\begin{pmatrix} c_{11} & c_{12} & c_{13} \\ c_{21} & c_{22} & c_{23} \\ c_{31} & c_{32} & c_{33} \end{pmatrix} = \frac{1}{Y}\begin{pmatrix} S_3T_2 - S_2T_3 & T_3 & -S_3 \\ S_1T_3 - S_3T_1 & -T_3 & S_3 \\ S_2T_1 - S_1T_2 & T_2 - T_1 & S_1 - S_2 \end{pmatrix},$$
$$Y = -S_3T_1 + S_3T_2 + S_1T_3 - S_2T_3. \tag{A5}$$

Case (c). Same material and geometry for both sub-layers

$$S_{1i} = \frac{1}{A_1}\left(\frac{c_{1i}}{k_1}\right), \quad i=1,2,3,$$
$$S_{2i} = \frac{1}{D_1}\left(\frac{c_{1i}S}{k_1} + \frac{c_{2i}}{k_2} + \frac{c_{3i}}{k_3}\right), \quad i=1,2,3,$$
$$S_{3i} = -\frac{1}{B_1}\left(\left(S+\frac{h_1}{2}\right)c_{1i} + c_{2i} + c_{3i}\right) - \frac{1}{D_1}\left(\frac{Sc_{1i}}{k_1^2} + \frac{c_{2i}}{k_2^2} + \frac{c_{3i}}{k_3^2}\right), \quad i=1,2,3,$$
$$S_{4i} = -\frac{1}{A_1}\left(\frac{c_{1i}}{k_1}\right), \quad i=1,2,3,$$
$$S_{5i} = -\frac{1}{D_2}\left(\frac{c_{1i}\left(S+\frac{h_1}{2}\right)}{k_1} + \frac{c_{2i}}{k_2} + \frac{c_{3i}}{k_3}\right), \quad i=1,2,3,$$
$$S_{6i} = \frac{1}{B_2}\left(\left(S+\frac{h_1}{2}\right)c_{1i} + c_{2i} + c_{3i}\right) + \frac{1}{D_2}\left(\frac{\left(S+\frac{h_1}{2}\right)c_{1i}}{k_1^2} + \frac{c_{2i}}{k_2^2} + \frac{c_{3i}}{k_3^2}\right), \quad i=1,2,3, \tag{A6}$$

where

$$k_1 = \sqrt{60G_{13}/E_{11}},$$
$$k_{2,3} = \sqrt{\frac{\frac{10E_{33}}{\kappa G_{13}} \pm \sqrt{\left((10E_{33}/\kappa G_{13})\right)^2 - (480E_{33}/E_{11})}}{2}},$$

$$S=\frac{-(h_1/2)k_1^4+((bK_nk_1^2h_1^3)/2)\left((1/B_1)+(1/B_2)\right)-((bK_n\left(h_1+h_2\right)h_1^4)/2D_2)}{k_1^4-b^2K_n\left((1/B_1)+(1/B_2)\right)k_1^2h_1^2+bK_n\left((1/D_1)+(1/D_2)\right)},$$

$$\begin{pmatrix} c_{11} & c_{12} & c_{13} \\ c_{21} & c_{22} & c_{23} \\ c_{31} & c_{32} & c_{33} \end{pmatrix}=\frac{1}{k_2-k_3}\begin{pmatrix} k_2-k_3 & 0 & 0 \\ -\left(k_1-k_3\right)S-\frac{h_1}{2}k_1 & -k_3 & -1 \\ \left(k_1-k_2\right)S+\frac{h_1}{2}k_1 & k_2 & 1 \end{pmatrix}. \tag{A7}$$